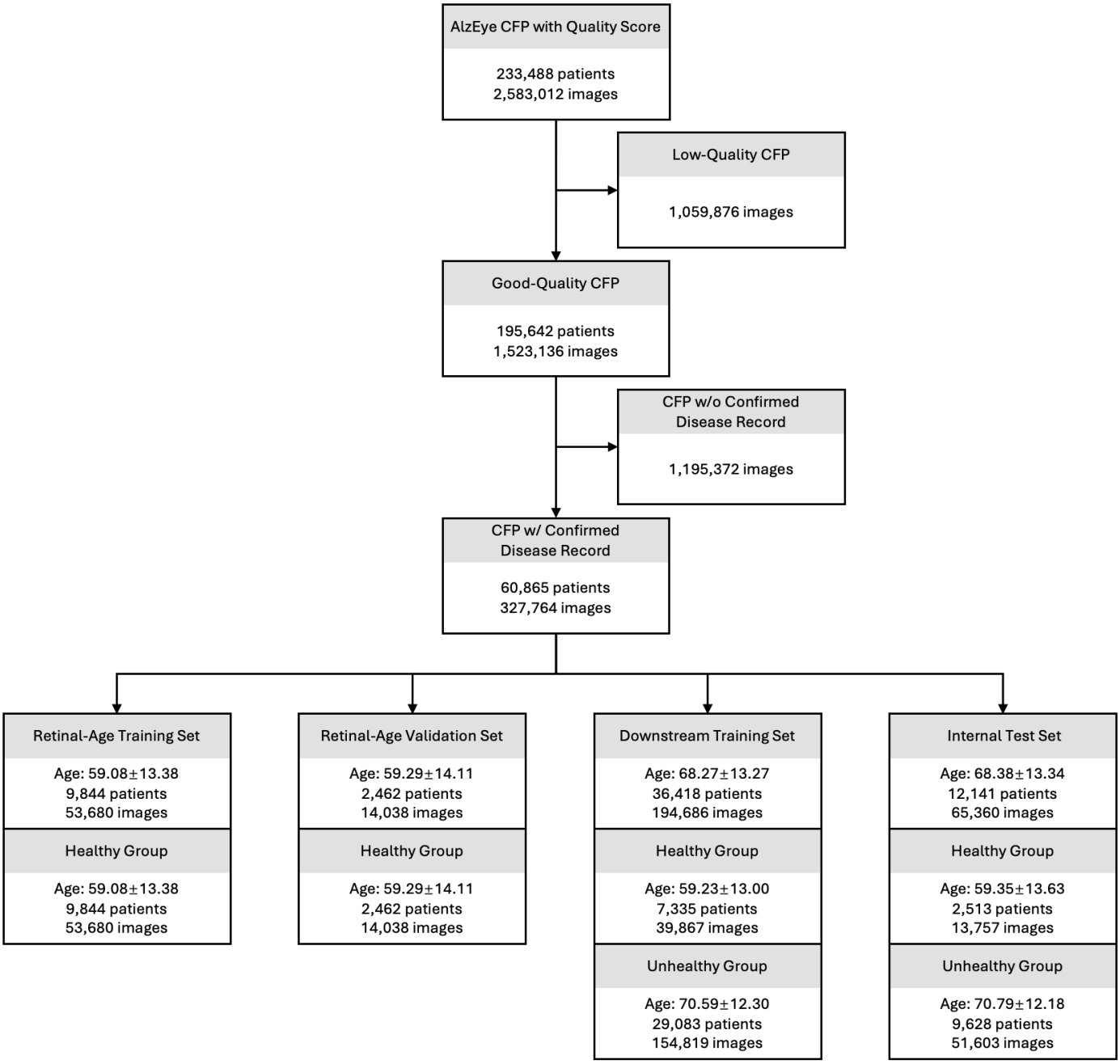

Supplementary Fig. 1. **Data curation for the AlzEye dataset.** CFPs were filtered for good quality and confirmed disease records. The dataset was then split at the patient level into four non-overlapping sets. The retinal-age training and validation sets (healthy group only) were used to train the retinal-age model and select its epoch. The downstream training set (healthy and unhealthy groups) was used to fit the age-calibrators and logistic regressions. The internal test set (healthy and unhealthy groups) was used for all internal evaluations.

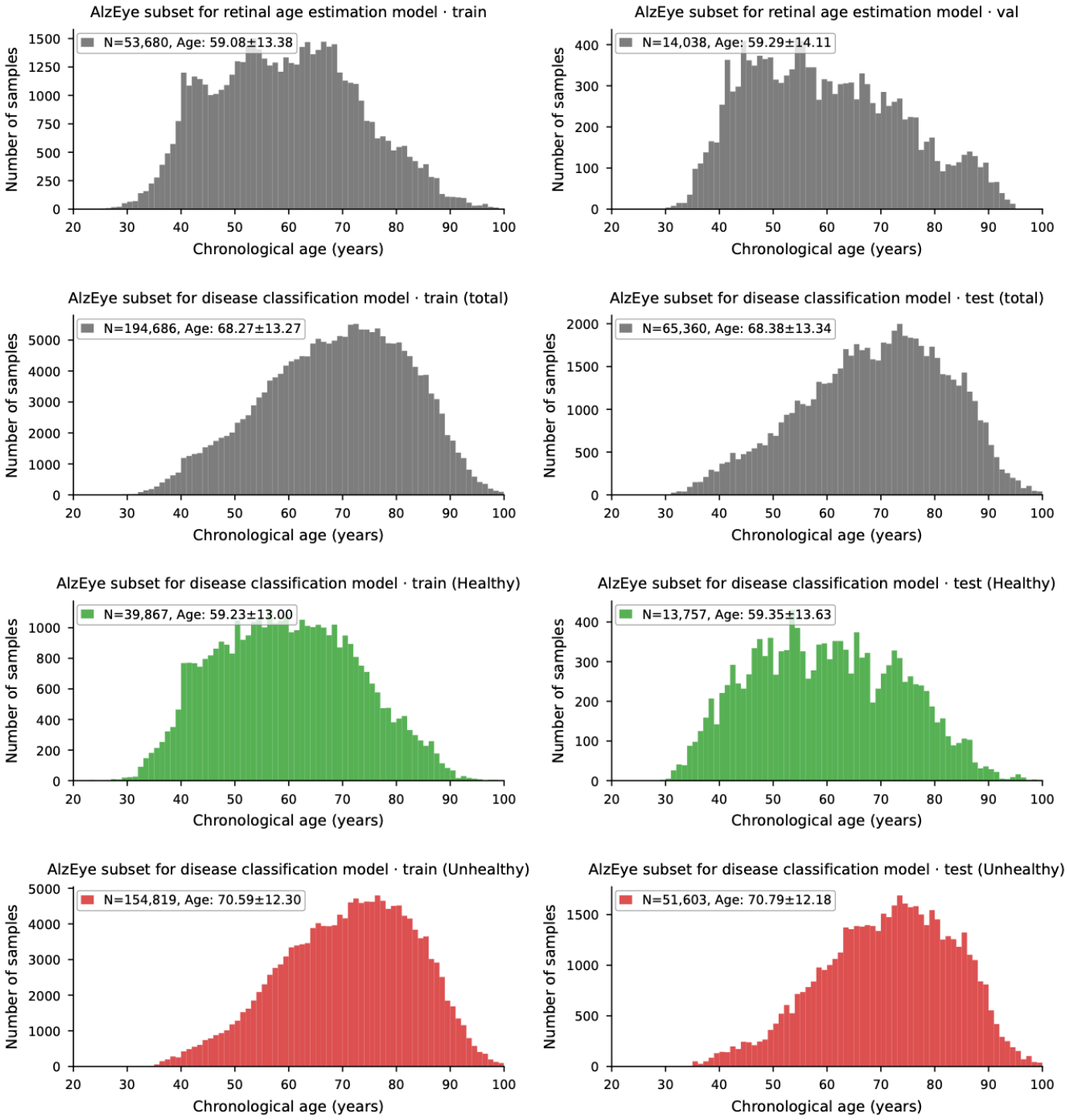

Supplementary Fig. 2. **Chronological-age distributions for each AlzEye set.** Distributions are shown for the four sets. For the downstream training set and the internal test set, the distributions of the healthy group and the unhealthy group are also shown separately.

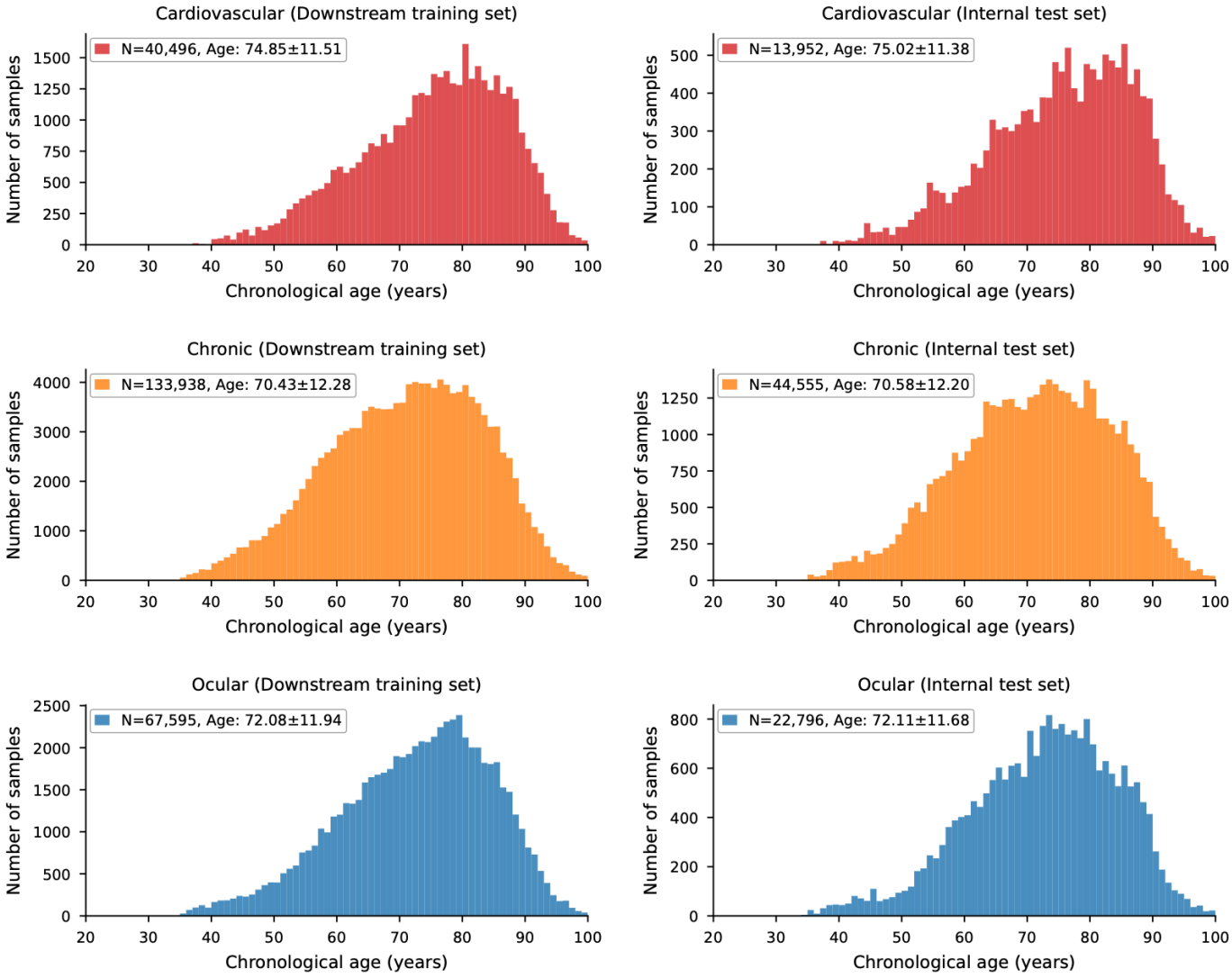

Supplementary Fig. 3. **Chronological-age distributions by disease category in AlzEye.** Distributions are shown for three disease categories (cardiovascular, chronic, and ocular), each in the downstream training set and the internal test set.

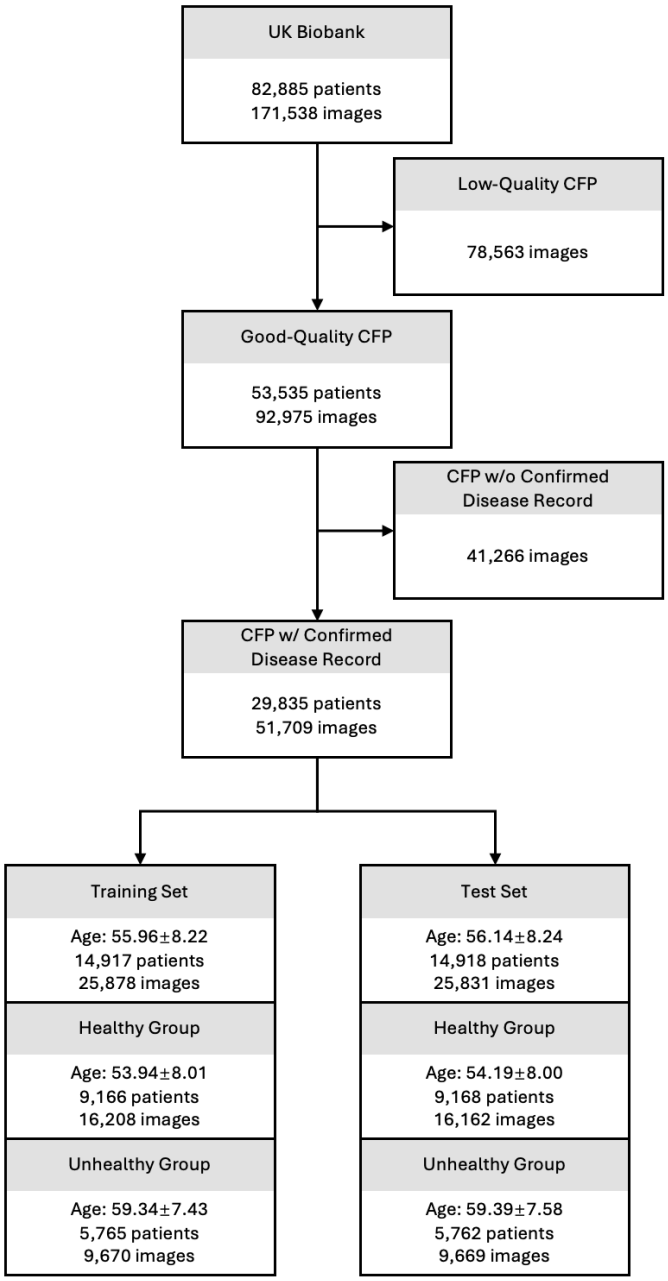

Supplementary Fig. 4. **Data curation for the UK Biobank dataset.** CFPs were filtered for good quality and confirmed disease records. The dataset was then split 50/50 at the patient level into a training set, used only for external calibration, and a test set, used only for evaluation.

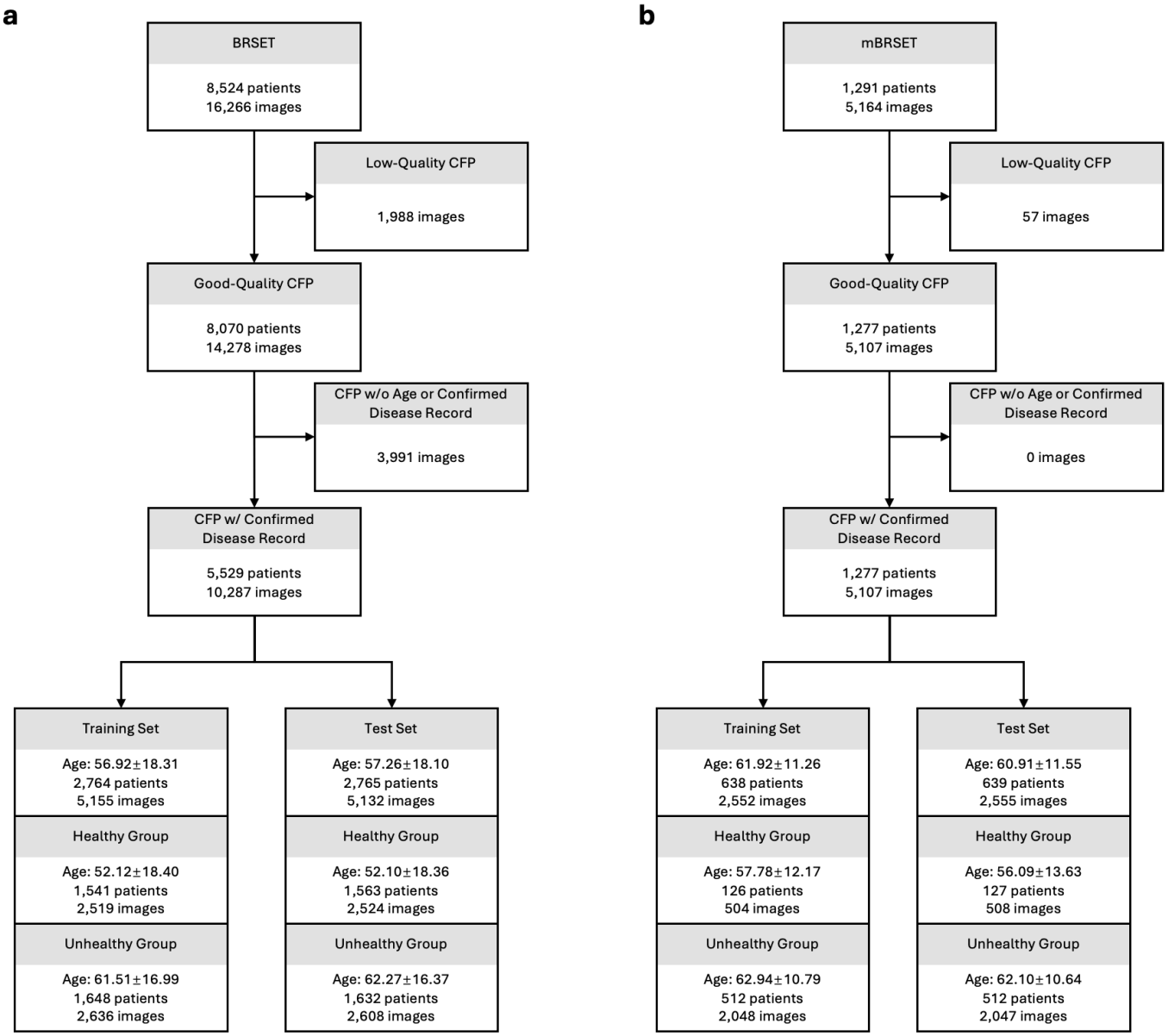

Supplementary Fig. 5. **Data curation for the BRSET and mBRSET datasets.** Each dataset was filtered for good quality and confirmed disease records, then split 50/50 at the patient level into a training set (used only for external calibration) and a test set (used only for evaluation). **a.** BRSET. **b.** mBRSET.

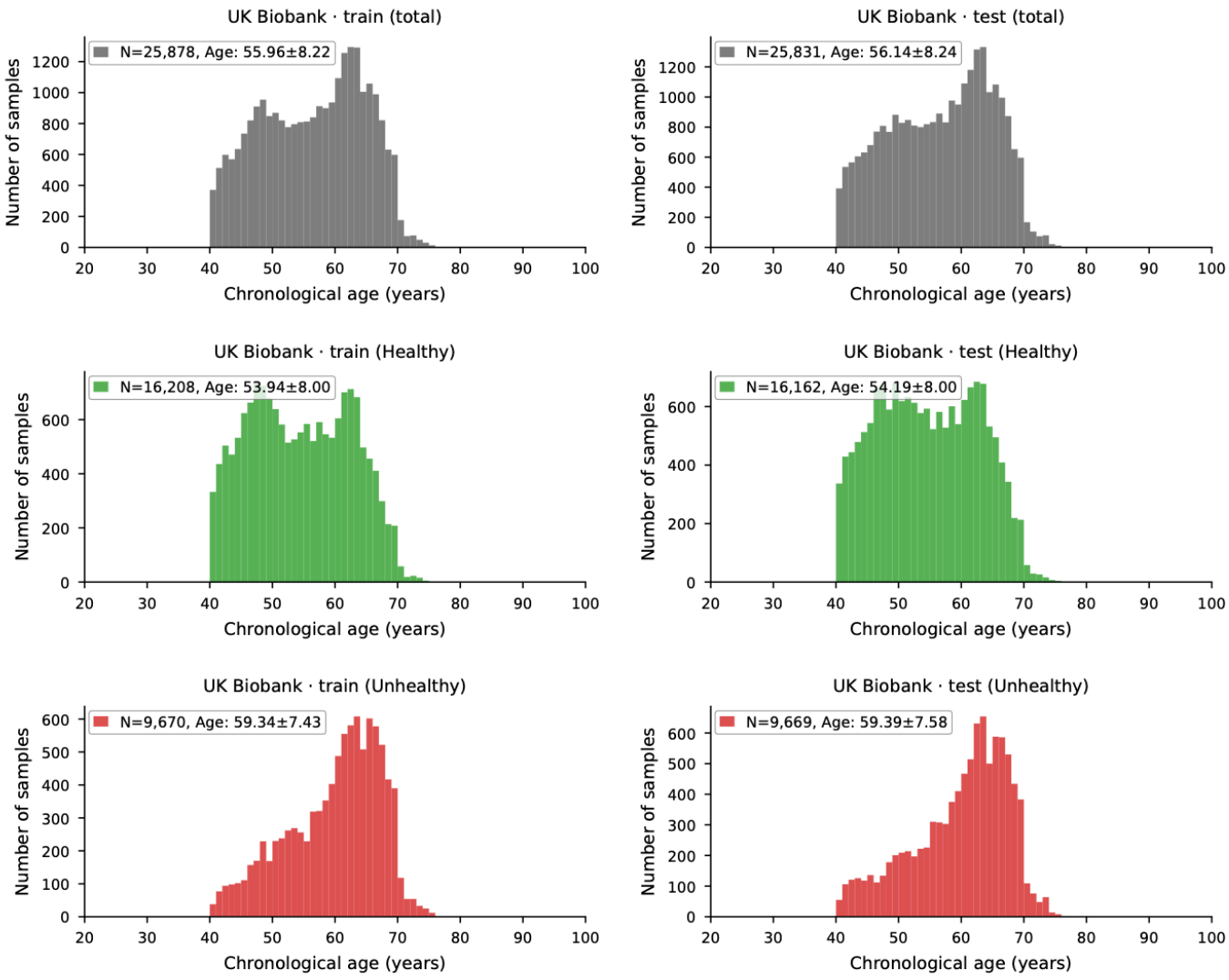

Supplementary Fig. 6. **Chronological-age distributions for the UK Biobank training and test sets.** For each set, the distributions of the total, the healthy group and the unhealthy group are shown.

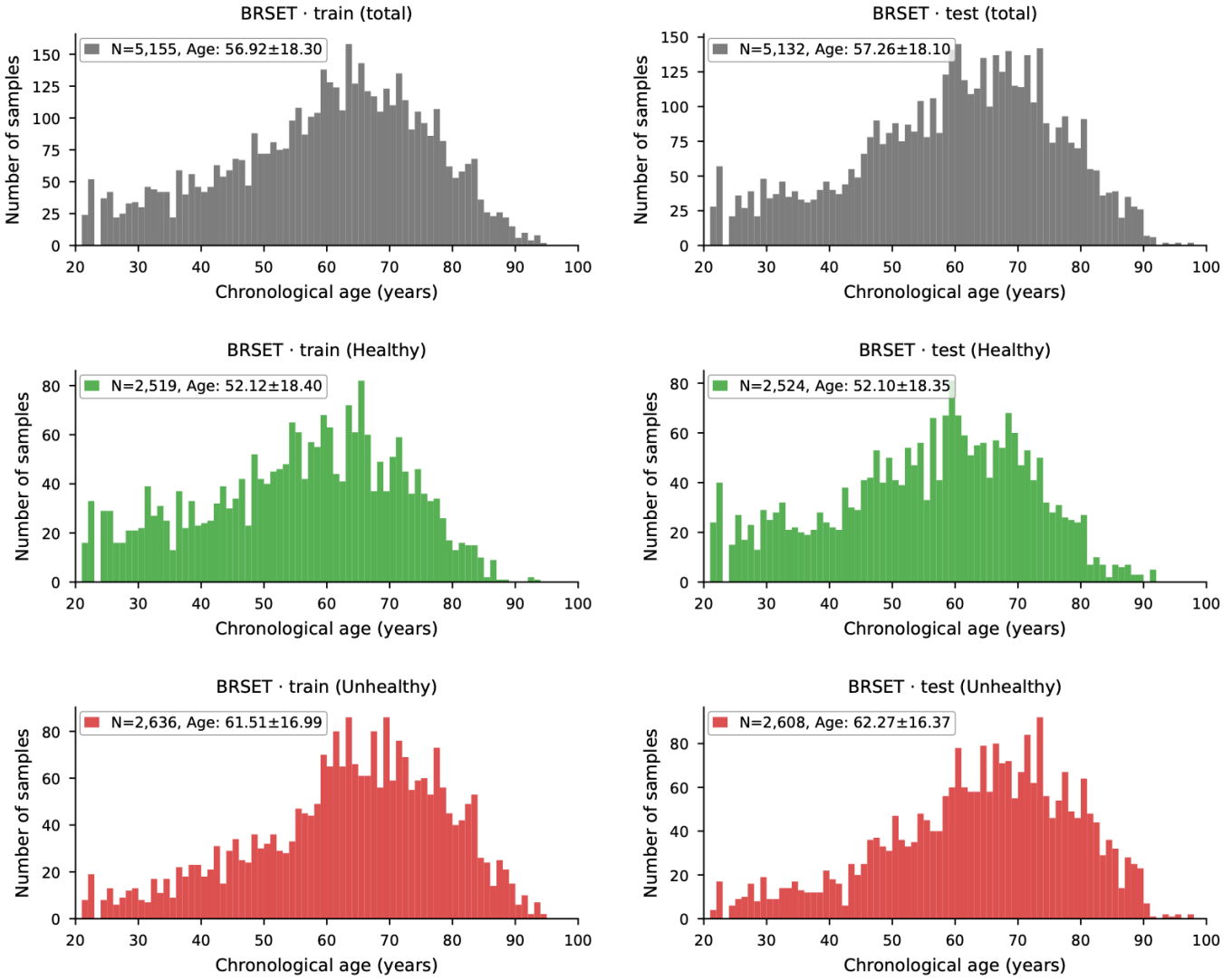

Supplementary Fig. 7. **Chronological-age distributions for the BRSET training and test sets.** For each set, the distributions of the total, the healthy group and the unhealthy group are shown.

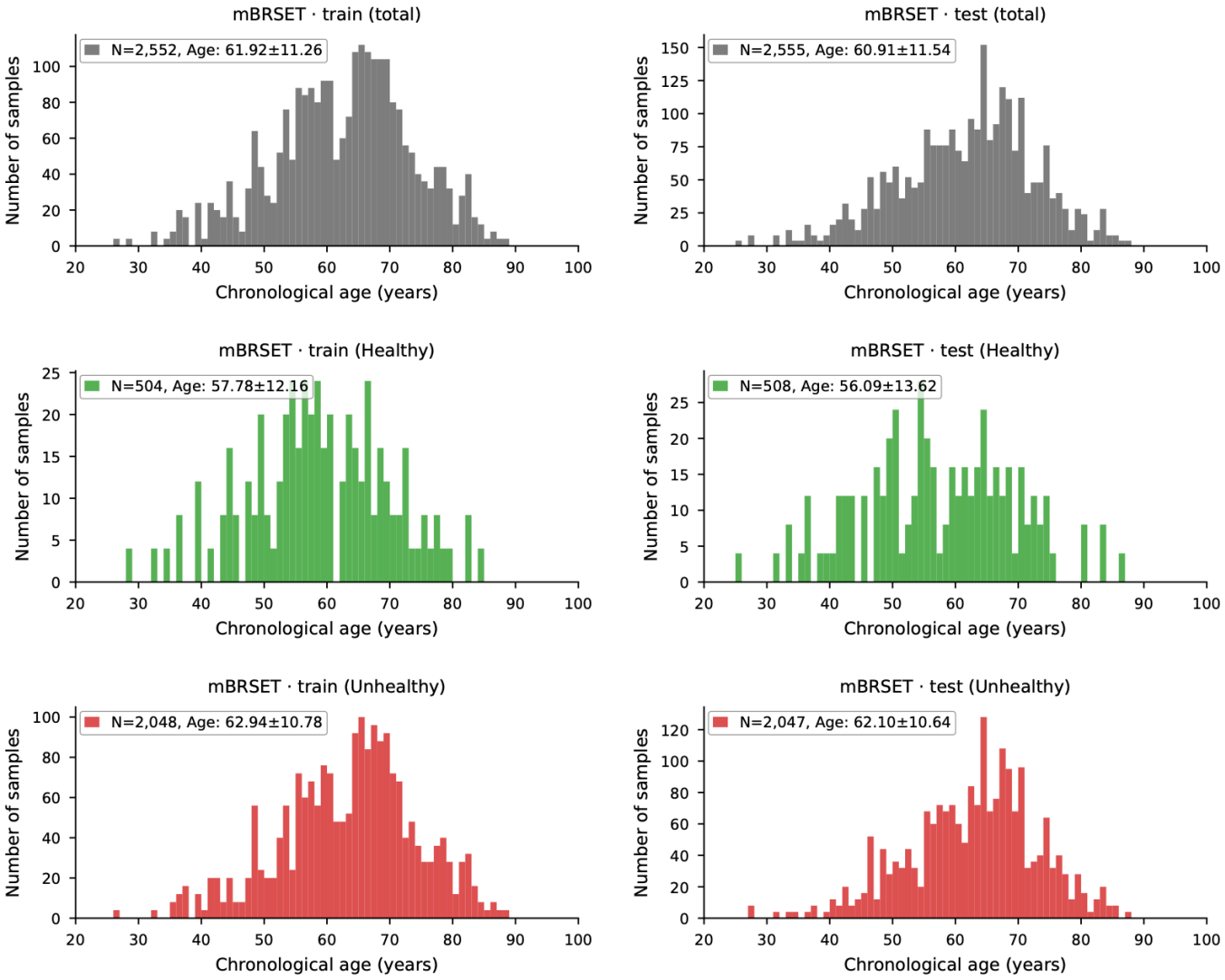

Supplementary Fig. 8. **Chronological-age distributions for the mBRSET training and test sets.** For each set, the distributions of the total, the healthy group and the unhealthy group are shown.

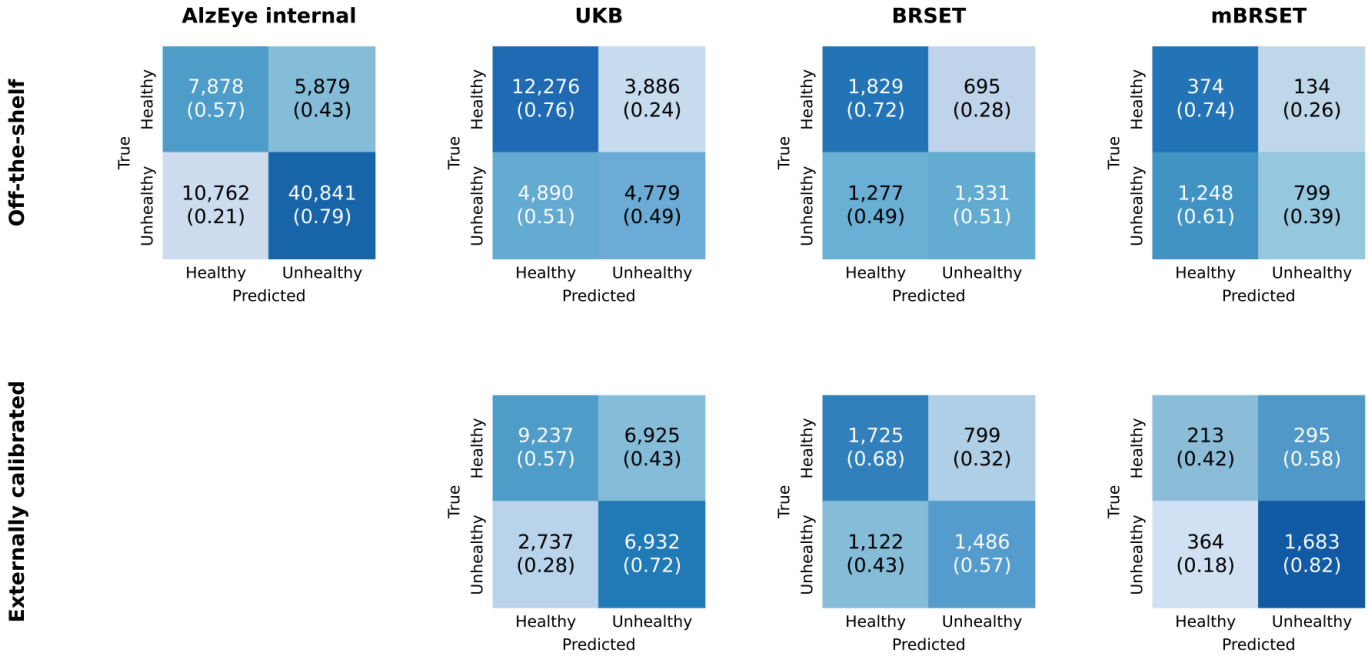

Supplementary Fig. 9. **Confusion matrices for unhealthy classification across cohorts.** Confusion matrices are shown for the Age + RAG + Age × RAG model at the image level, for the AlzEye internal test set and three external cohorts (UK Biobank, BRSET, mBRSET), under off-the-shelf (top row) and externally calibrated (bottom row) evaluation. The AlzEye internal test set is shown in the off-the-shelf row only. Rows are the true label and columns the predicted label; each cell gives the image count with the row-normalised proportion in parentheses.

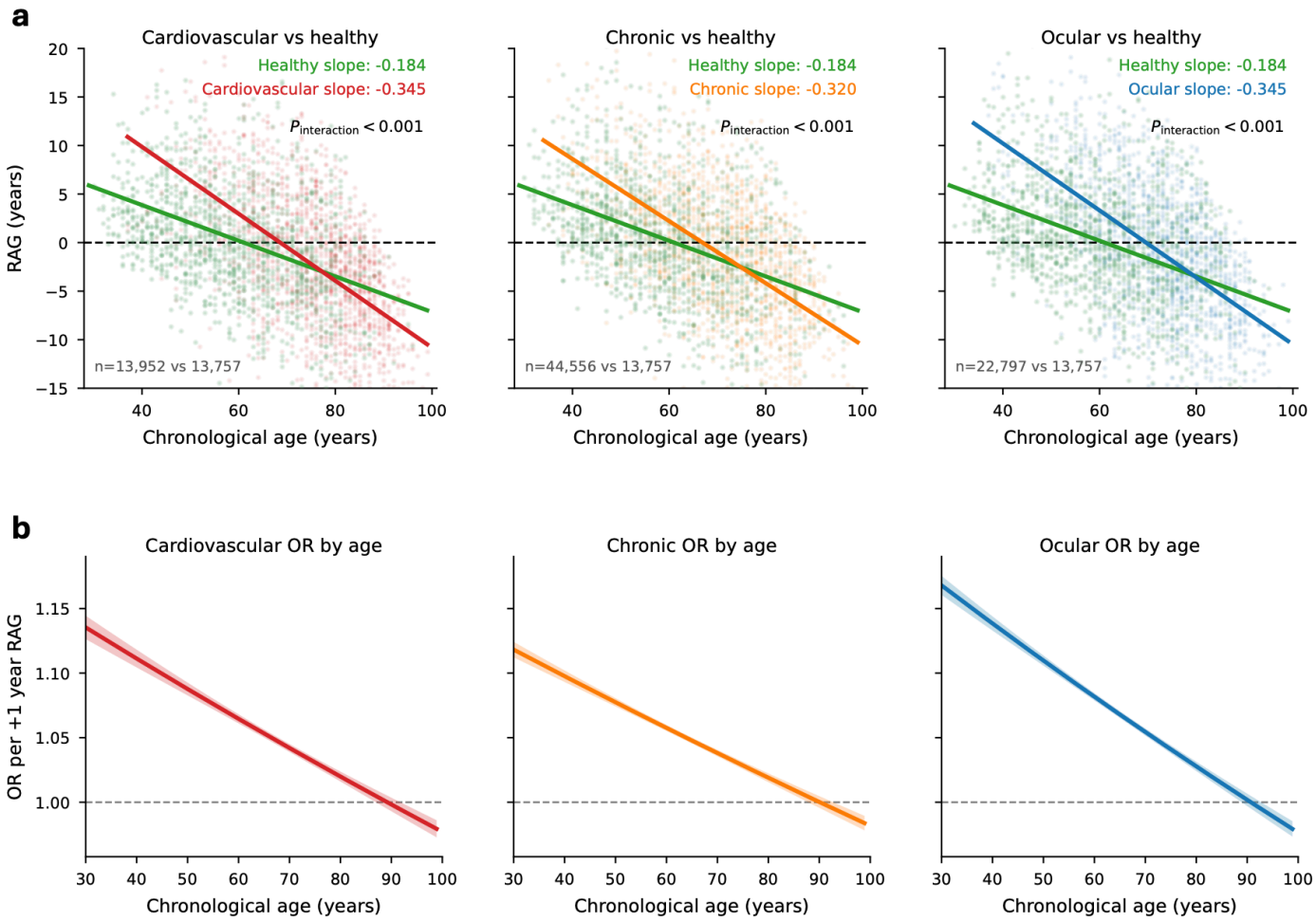

Fig. 10. **Disease-specific differential RTM and age-dependent RAG associations on the AlzEye internal test set**. **a.** Linear regression of RAG on chronological age, disease group, and their interaction, shown separately for cardiovascular, chronic, and ocular groups versus the healthy group. The healthy group was used as the common reference group in each comparison. All three disease groups show steeper negative RAG-age slopes than the healthy group, with significant Age × Group interactions (all interaction p<0.001 from Wald tests). **b.** Age-specific odds ratios for each disease category per 1-year increase in RAG, estimated from the Age + RAG + Age × RAG logistic model. Shaded bands denote 95% CIs. The declining odds-ratio curves show that the association between RAG and disease status is strongly age-dependent, with larger positive associations at younger ages and attenuation toward older ages. Full results are reported in Supplementary Tab. 5,8.

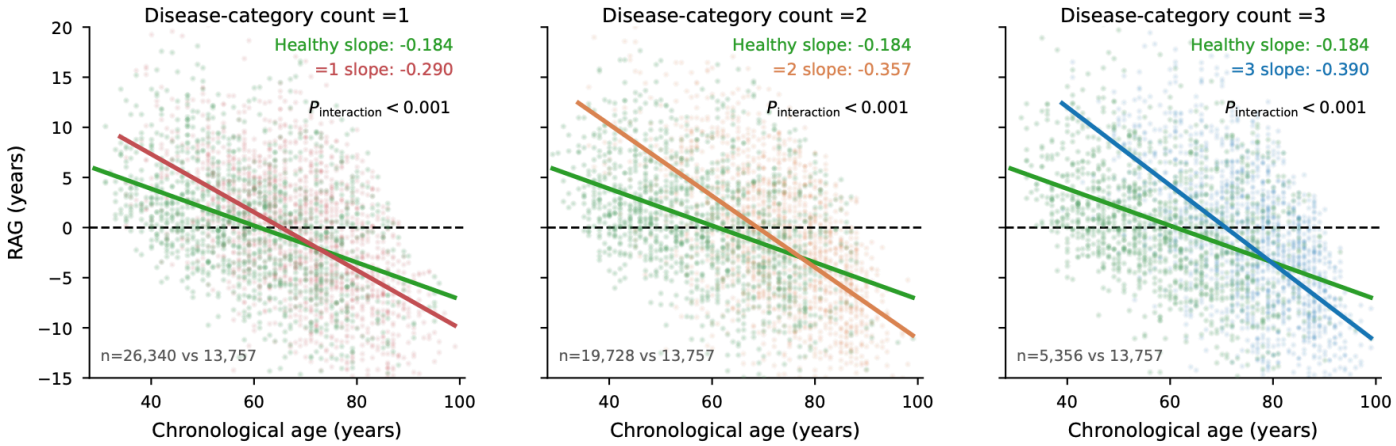

Fig. 11. **Differential RTM by disease-category count on the AlzEye internal test set.** Linear regression of RAG on chronological age, exact disease-category count group, and their interaction, shown separately for participants with exactly 1, 2, or 3 disease categories versus healthy controls. The healthy group was used as the common reference group in each comparison. Full results are reported in Supplementary Tab. 5.

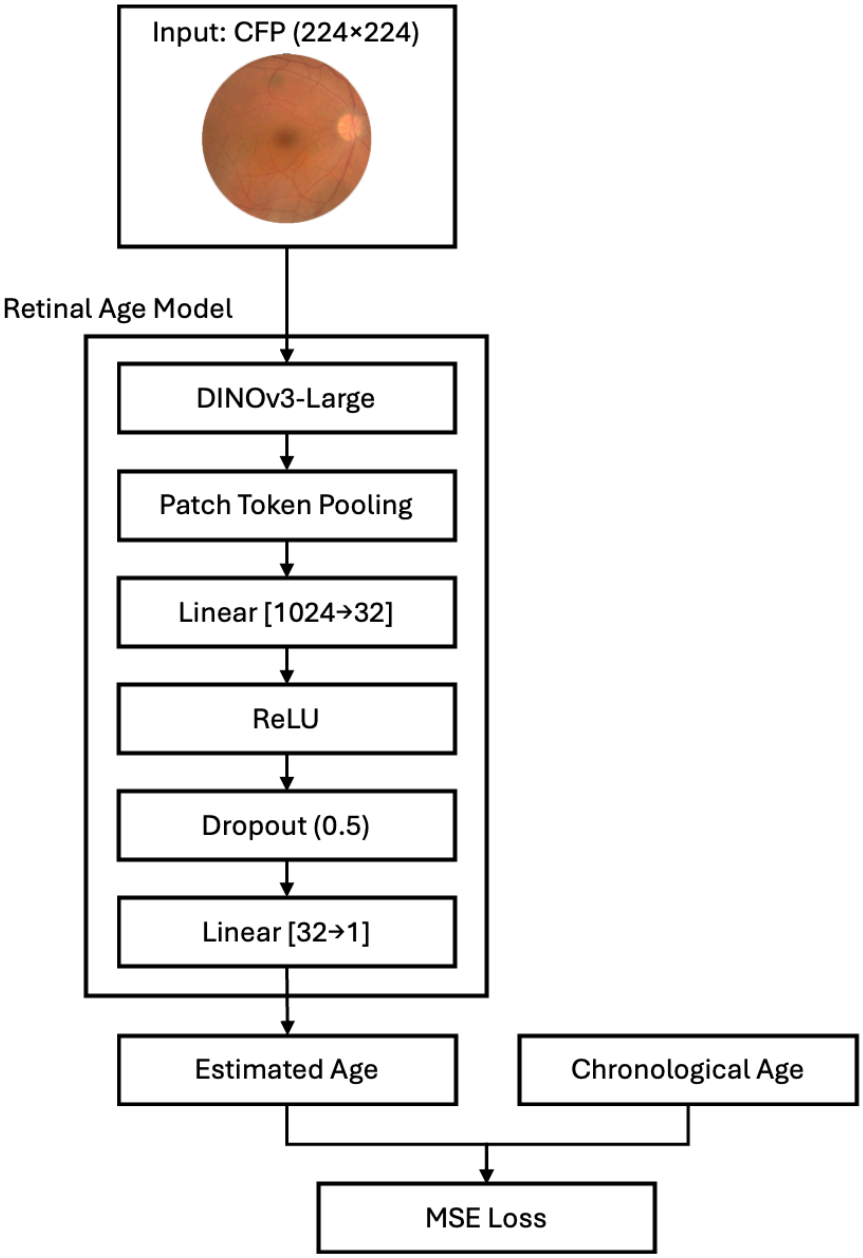

Supplementary Fig. 12. **Retinal age model architecture.** A CFP image resized to 224×224 pixels was used as input to the retinal age model. The image was encoded using a DINOv3-Large vision transformer backbone, followed by patch token pooling and a two-layer regression head to output estimated retinal age. The model was fine-tuned end-to-end against chronological age using mean-squared-error (MSE) loss.